







## Article

# Nonlinear Dual-Wavelength Switching of Ultrashort Pulses in Slightly Asymmetric Dual-Core Fibers

Mattia Longobucco<sup>1,2,3,\*</sup>, Ignas Astrauskas<sup>4,5</sup>, Audrius Pugžlys<sup>4</sup>, Andrius Baltuška<sup>4</sup>,  
Ryszard Buczyński<sup>1,2</sup> and Ignác Bugár<sup>4,6,\*</sup>

- <sup>1</sup> Department of Glass, Łukasiewicz Research Network—Institute of Microelectronics and Photonics, Aleja Lotników 32/46, 02-668 Warsaw, Poland; ryszard.buczynski@fuw.edu.pl  
<sup>2</sup> Department of Photonics, Faculty of Physics, University of Warsaw, Pasteura 5, 02-093 Warsaw, Poland  
<sup>3</sup> School of Electrical and Electronics Engineering, Nanyang Technological University, 50 Nanyang Avenue, Singapore 639798, Singapore  
<sup>4</sup> Photonics Institute, TU Wien, Gußhausstraße 27-387, 1040 Vienna, Austria; ignas.astrauskas@lightcon.com (I.A.); audrius.pugzlys@tuwien.ac.at (A.P.); andrius.baltuska@tuwien.ac.at (A.B.)  
<sup>5</sup> Light Conversion, Keramikų St. 2B, 10233 Vilnius, Lithuania  
<sup>6</sup> Institute of Chemistry and Environmental Sciences, University of Ss. Cyril and Methodius in Trnava, Nám. J. Herdu 2, 917 00 Trnava, Slovakia  
\* Correspondence: mlongobucco@fuw.edu.pl (M.L.); ignac.bugar@tuwien.ac.at (I.B.)

## Abstract

We conducted a comprehensive experimental investigation of dual-wavelength switching of 1560 nm, 75 fs pulses (referred to as *signal*) driven by 1030 nm, 270 fs pulses (referred to as *control*) using two dual-core fibers with high refractive index contrast and different levels of asymmetry. The study explores the influence of fiber length, control pulse energy, and control-signal pulse delay on switching performance. For the fiber with higher dual-core asymmetry, we achieved an exceptional switching contrast of 41.6 dB at a 14 mm fiber length, exhibiting a homogeneous character within the spectral range of 1450–1650 nm. In contrast, the study of the weaker dual-core asymmetry fiber revealed a maximum switching contrast of 10.7 dB at a 22 mm fiber length, albeit under lower control pulse energy. These observations confirm that the switching mechanism is based on the nonlinear balancing of dual-core asymmetry, wherein the control pulse induces an enhancement of the effective refractive index in the fast fiber core, facilitating the switching of the signal pulse. This work demonstrates high switching contrasts with only a 0.4–0.6 nJ control pulse energy requirement, providing experimental confirmation of a previously reported theoretical model. For the first time, the dual-wavelength switching performance of dual-core fibers with varying levels of asymmetry is compared. The results reveal key directions for the further development of dual-core fibers in view of their potential applications.

**Keywords:** dual-core optical fibers; soft glass optical fibers; nonlinear fiber optics; all-optical switching; asymmetric coupler



Academic Editor: Martin J. D. Clift

Received: 1 August 2025

Revised: 30 September 2025

Accepted: 28 October 2025

Published: 30 October 2025

**Citation:** Longobucco, M.; Astrauskas, I.; Pugžlys, A.; Baltuška, A.; Buczyński, R.; Bugár, I. Nonlinear Dual-Wavelength Switching of Ultrashort Pulses in Slightly Asymmetric Dual-Core Fibers. *Fibers* **2025**, *13*, 146. <https://doi.org/10.3390/fib13110146>

**Copyright:** © 2025 by the authors. Licensee MDPI, Basel, Switzerland. This article is an open access article distributed under the terms and conditions of the Creative Commons Attribution (CC BY) license (<https://creativecommons.org/licenses/by/4.0/>).

## 1. Introduction

Ultrafast all-optical signal processing stands out as a compelling research area in the information technology domain [1]. Within the realm of optical communication technology [2], a diverse set of devices, including all-optical switches [3], multiplexers [4], demultiplexers [5], and routers [6], represents crucial components enabling digital operations at bit rates that exceed Tbit/s [7,8]. Among digital operations in the optical domain,

arithmetic and logic operations are prevalent [9–11], with a focus on all-optical switching as a key investigation area [1,12]. The indispensability of all-optical switches extends to applications such as optical buffers [13], wavelength division multiplexed interconnects [14], and data center networks [15]. Often, nonlinear optical processes govern the operation of optical switches and digital devices, utilizing phenomena like the Kerr effect [16], inverse Raman scattering [17], and four-wave mixing [18]. The nonlinear directional coupler approach, based on intensity-induced Kerr refractive index changes and introduced in the early 1980s, was later refined through the consideration of highly nonlinear dual-core fibers (DCFs) [19]. Several ultrafast studies have investigated DCFs with enhanced nonlinearity to demonstrate low-pulse-energy all-optical switching for optical signal processing applications. One of the first attempts employed a photonic-crystal-based DCF of approximately 1 cm length, excited through C-band 120 fs pulses, but achieved only partial switching performance [20]. More recently, chalcogenide [21] and tellurite glass [22] have been studied using 1.4 ps and 220 fs excitation pulses, respectively; however, both approaches required relatively long fibers on the order of 10 cm. In addition, the fibers in these works were fabricated by side-fusing two identical fibers, introducing additional technical complexity, and only low-contrast switching was demonstrated. All of the above studies also reported substantial nonlinear spectral broadening of the guided pulses as a byproduct of Kerr-nonlinearity-driven switching, which compromises the integrity of the output pulses and limits their potential for subsequent processing.

In addition to the motivation to demonstrate a nonlinear directional coupler through a cost-effective approach, DCF technology has been significantly developed due to its promising applications in other domains. Examples of DCF-related research achievements include all-fiber integrated immunosensors [23], flat-gain fiber-optical parametric amplifiers [24], and electrically switchable nanomechanical fiber couplers [25]. In the context of cross-connect all-optical switching, alternative techniques such as metamaterial-based devices [26], ring resonators [27], plasmonic waveguides [28], and nonlinear optical loop mirrors [29] have been explored. However, the simplicity of fabricating and cascading DCFs makes them more favorable than these alternatives, as they inherently possess two interaction channels, eliminating the need for duplication and additional input signal splitters, thereby reducing cost and complexity.

High-contrast all-optical switching has recently been demonstrated in 40 cm-long DCFs excited by 0.5 ns, 1040 nm signal pulses, controlled via counter-propagating, identical-wavelength control pulses with microjoule-level energies [30,31]. These studies, which explore beam manipulation in multimode and multicore fibers, represent an important step toward practical, coherent optical computing with potential for multichannel functionality. However, the relatively long fiber lengths and high pulse energies indicate a need for more compact and energy-efficient solutions—an issue addressed in our recent studies employing highly nonlinear multicomponent-glass DCFs. A further advantage of our approach is the use of a dual-wavelength switching scheme, enabling control pulses that are 3–4 times longer in duration than the signal pulses. By exciting a single core with 1030 nm control pulses and 1560 nm signal pulses, and optimizing the control pulse energy and delay, we achieved efficient signal switching between the excited and non-excited cores with minimal distortion [32,33]. This configuration facilitates the straightforward separation of the two fields not only spectrally but also spatially, as only the signal pulse couples to the cross core. Moreover, the technique is inherently broadband, with nearly identical switching performance obtained across the entire C-band. Exciting a single core with 1030 nm control and 1560 nm signal pulses and controlling the energy and delay of the control pulse, effective switching of the signal pulse between the excited and non-excited cores was established with limited distortions. The thorough matching of the two fields in

both the spatial and temporal domains enabled the high-contrast switching performance above 20 dB, applying sub-nanojoule control pulse energies. This novel technique supports all-optical signal processing schemes with potential processing rates exceeding 2 Tbit/s, limited primarily due to control pulse duration and walk-off of 152 fs between the signal and control pulses. The initial experiments performed on DCFs, which were not optimized for the dual-wavelength switching, along with dedicated numerical simulations, indicate potential in switching energy reduction and an improved processing rate. Here, we study the dual-wavelength switching approach in the second-generation high-index contrast soft glass DCF, designed with the aim of reducing dual-core (DC) asymmetry, a critical factor influencing switching energy. We analyze the performance of the observed switching and compare it with that of the first-generation DCF.

In this paper, we present a detailed, comparative, experimental study of dual-wavelength switching using both the first- and second-generation specialty DCFs, focusing on control pulse energy, fiber length, and signal-control pulse synchronization. The recent study enables the investigation of the impact of DC asymmetry on switching performance, achieving high contrasts at low input powers and confirming a previously reported theoretical model [33]. Our findings offer new insights into the role of fiber design in enhancing switching efficiency and advance the understanding of ultrafast all-optical switching mechanisms based on combined DC, dual-wavelength nonlinear cross-interactions.

## 2. Theory and Methods

The dual-wavelength cross-switching strategy is more effective than the previous ultrafast solitonic self-switching methods utilizing the same type of DCF [34–36] because it mitigates the disadvantageous effect of DC asymmetry. This asymmetry arises during the stack-and-draw fabrication process, leading to distinguishable slow and fast cores with effective refractive indices  $n_{\text{eff},s}$  and  $n_{\text{eff},f} < n_{\text{eff},s}$ , respectively [32,36]. In the linear propagation regime, asymmetry inhibits the self-switching of ultrashort pulses, resulting in only a partial transfer of energy from the excited core to the non-excited core. It has been confirmed both theoretically and experimentally that optical asymmetry can exert a beneficial effect on switching performance when it is nonlinearly compensated within the framework of DC soliton dynamics. However, this compensation requires the evolution of a high-order soliton, which is inherently lossy and introduces unwanted distortions to the information-carrying ultrashort pulse. In contrast, the dual-wavelength switching approach avoids both of these drawbacks and performs effectively at typical asymmetry levels of approximately  $10^{-4}$ , defined as  $n_{\text{eff},s} - n_{\text{eff},f}$ . In this case, the elimination of the asymmetry is relatively easy via launching a control pulse into the fast core with a proper level of peak intensity, which increases the  $n_{\text{eff},f}$  to the level of the  $n_{\text{eff},s}$  via Kerr nonlinearity. If the co-propagation of an appropriate control pulse with a significantly shorter signal pulse is ensured, the signal pulse passes through a symmetric coupler and, therefore, is transferred to the cross core with high effectiveness. The last condition of such an advantageous switching scheme is that the control pulse should involve a negligible transfer to the cross core, even in the case of balanced asymmetry, which is fulfilled if its wavelength is shorter than that of the signal pulse. The strong spectral dependence of the coupling length of common DCFs enables the achievement of this condition via down-tuning the control-pulse wavelength by several 100 nm.

The experimental setup has already been presented in detail in [32], and its schematics are reported in Figure 1. It consists of two arms devoted to two femtosecond pulse sequences with different wavelengths generated at a 10 kHz repetition rate, labeled as follows:

- **Control:** 1030 nm, 270 fs pulse from a commercial ultrafast Yb:KGW amplifier (Pharos, Light Conversion, Vilnius, Lithuania);

- **Signal:** 1560 nm, 75 fs pulse generated in a double-pass optical parametric amplifier (OPA) and pumped via a second harmonic of the same Yb:KGW amplifier.

The two pulses were combined using a dichroic mirror and time-synchronized through a delay line unit positioned in the control arm. Independent control over the energy and polarization of the control pulses was achieved by employing a variable attenuator consisting of two half-wave plates separated by a Glan–Taylor polarizer. The energy of the signal beam was set to 0.1 nJ to ensure its linear propagation in the absence of the control beam. A two-lens telescope in the signal arm was employed to maintain identical diameters for both beams at the fiber input. In-coupling into a single core and the out-coupling of the beams from both cores were facilitated via two 40× microscope objectives. The output facet of the DCF was monitored via an infrared camera placed in the image plane of the output objective, while the spectrum was recorded using a NIRQuest512-2.5 spectrometer, Ocean Optics, Stuttgart, Germany (900–2500 nm spectral range,  $\approx 6.3$  nm FWHM resolution with the selected slit/grating configuration) connected through a multimode fiber. The fiber end was sequentially aligned with the images of the two cores to separately record the spectra originating from each core. The corresponding camera image was captured by tilting a flip mirror positioned before the image plane of the output objective. The control field was suppressed behind the fiber via a dichroic mirror, which reflected the 1030 nm control wavelength while transmitting the 1560 nm signal, ensuring that only the signal field was directed to the spectrometer and infrared camera for characterization. The coupling length of the control field at 1030 nm is extremely long compared to the fiber length used in this work (approximately 20.9 m for the second-generation fiber), so that virtually no power is transferred to the adjacent core over the 14 mm sample. Further details on the experimental setup, ensuring femtosecond excitation and output field registration using identical DCF, can be found in references [32,34]. As previously discussed in [32], the excitation of the fast core supports more efficient switching compared to the slow core excitation, thanks to the DC asymmetry-balancing principle. Consequently, this paper exclusively presents results related to the fast core excitation via both pulses of different wavelengths.

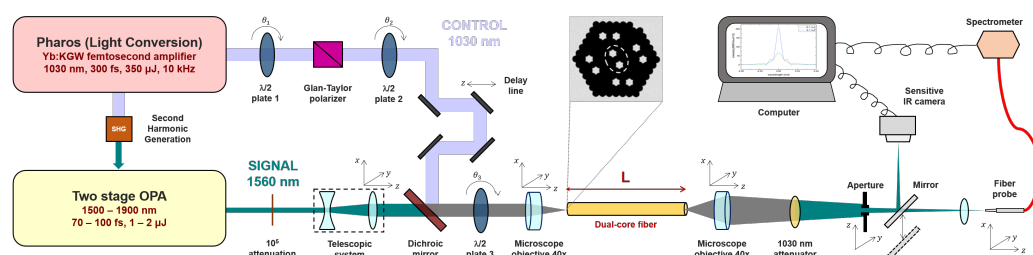


**Figure 1.** Experimental setup schematics showing the laser source for synchronized control and signal pulses, the configuration for controlled DCF excitation, and the system for output signal detection.

### 3. Experimental Results

#### 3.1. Fiber Length Dependence

We first used the DCF of the first generation (FG-DCF) with the cross section as shown in Figure 2. The fiber is made of two thermally matched soft glasses: lead silicate (PBG-08) and borosilicate (UV-710) for the cores and cladding, respectively, and has a DC asymmetry level  $\delta_a = 2.2 \times 10^{-4}$ , at 1560 nm. It was determined via numerical simulations based on real fiber cross section and glass properties as the difference between the refractive indices of the slow and fast cores,  $\delta_a = n_{\text{eff},s} - n_{\text{eff},f}$  respectively [35,36]. A series of camera images of the spatial distribution of the signal field was recorded with increasing control pulse energy in the range of 0.1–4 nJ. The control field was blocked behind the fiber by a dichroic

mirror. Under unchanged experimental conditions, the spectra of signal pulses coming out from the excited and non-excited cores were also separately recorded.

To identify the optimal fiber length for dual-wavelength switching performance, the registrations described above were repeatedly performed through a sequential cut-back of the DCF. The fiber was cut in the range of 18–10 mm with 2 mm steps. The key parameter of the switching performance is the minimal DC extinction ratio (MER), calculated in the dB scale as follows:

$$MER(E_{in}) = \min \left\{ 10 \cdot \log \left[ \frac{E_{exc}(E_{in})}{E_{ne}(E_{in})} \right] \right\}, \quad (1)$$

where  $E_{exc}$ ,  $E_{ne}$ , and  $E_{in}$  are the output signal energy from the excited (fast) and non-excited (slow) cores and the input control pulse energy at the fiber input (considering a fiber coupling coefficient of 50% [32]), respectively. The output energies were determined via the integration of the intensity values of all the pixels of the camera images in the vicinity of the excited and non-excited cores, respectively. If the extinction ratio is negative, it indicates that the output energy is higher in the case of the non-excited (cross) core. Therefore, the lower the MER, the more efficient the switching performance, indicating that the transfer of the signal pulse between the cores is more efficient. Figure 2 illustrates the dependence of the MER on the fiber length ( $L$ ), with the inset showing a scanned electronic microscope (SEM) image of the DCF cross section used in the experiment. Across all fiber lengths analyzed, the MER values are consistently negative, indicating the reliable occurrence of a dominance exchange between the cores under an increasing control pulse energy. Notably, the extreme MER value of  $-9.1$  dB was observed at a 14 mm fiber length.

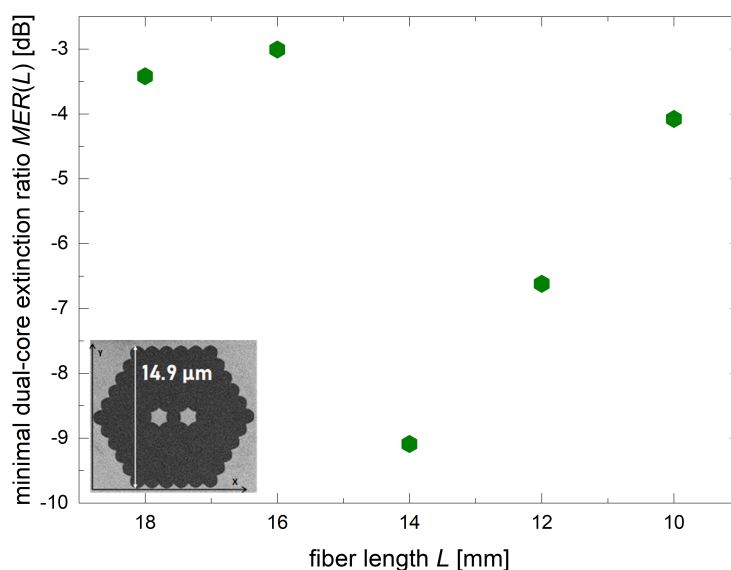


**Figure 2.** Dependence of the minimal extinction ratio (MER) at optimal control pulse energy, applying the dual-wavelength switching approach for each analyzed length of the first generation DCF with cross section as inset.

Comparing our findings with those reported in [32], where an optimal length of 14 mm was identified using a nearly identical DCF, we obtained similar results. Camera images of the fiber output facet recorded at 14 mm are shown in Figure 3. These images reveal a reversible transition in core dominance—from the top (excited) core to the bottom (non-excited) core—occurring in the control pulse energy ranges of 0.14–0.6 nJ and 0.6–1.2 nJ, which represent the cross- and reversal-switching regimes, respectively. The MER was identified at 0.6 nJ. To comprehensively characterize the switching performance, additionally, the maximal switching contrast (MSC) was calculated. This value is obtained by subtracting

the highest and lowest values of the extinction ratio in one energy-dependent series. In the case of the camera images shown in Figure 3, the MSC is 41.6 dB, obtained by subtracting extinction ratios at 0.21 nJ and 0.6 nJ control pulse energies, where maximal intensity dominance in the excited and non-excited cores was, respectively, recorded. Notably, the energy at which the best switching performance with a minimal extinction ratio occurs (referred to as the switching energy) is approximately 6 times lower than identified in the optimal case reported in [32]. Thus, we achieved significant improvement with reduced energy requirements for the control pulse and higher switching contrast, representing a further step toward highly efficient, low-energy-consumption, all-optical switching.

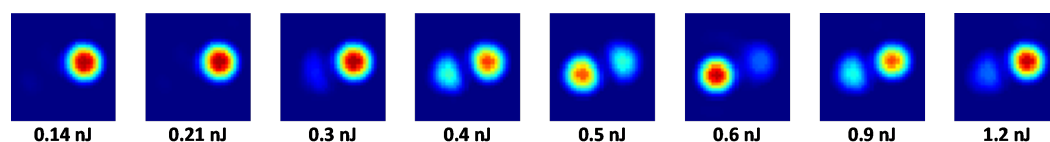


**Figure 3.** Infrared camera images of the output field of the 1560 nm, 75 fs signal pulse at 14 mm DCF with cross section as shown in Figure 2, under increasing energy of 1030 nm, 270 fs control pulse.

To achieve a complete characterization of the switching performance, we calculated the spectrally resolved DC extinction ratio as  $ER(\lambda, E_{in}) = 10 \cdot \log[S_{exc}(\lambda, E_{in})/S_{ne}(\lambda, E_{in})]$ .  $S_{exc}(\lambda, E_{in})$  and  $S_{ne}(\lambda, E_{in})$  are the separately recorded spectra at the outputs of the excited and non-excited core, respectively, at each input energy level,  $E_{in}$ , corresponding to the camera images in Figure 3. Figure 4 shows the spectrally resolved  $ER$  in the spectral window of 1450–1650 nm. The results reveal that, in the case of the control pulse energies of 0.14–0.3 nJ, the  $ER$  achieves positive values in the entire spectral window, indicating that the pulse is mostly confined to the excited core. In the case of 0.4 nJ control pulse energy (cyan curve), the  $ER$  is positive in the blue side of the spectrum and negative on the red side. The curves obtained at 0.5 and 0.6 nJ control pulse energy are entirely located on the negative  $ER$  side of the graph, meaning that all frequency components of the signal pulse have efficiently switched from the excited to the cross core (cross-switching). The  $ER$  at 0.9 and 1.2 nJ control pulse energy are again located in the positive half of the graph; this finding reveals that the signal pulse is again confined to the excited core (reversal switching). The spectral results shown in Figure 4 are consistent with the camera images presented in Figure 3; the reversible dominance exchange between the two cores was observed at the same control pulse energies using both measurement techniques. Furthermore, we calculated the spectrally resolved SC, defined as the difference between the  $ER$  curves, and identified three wavelengths at which the SC is maximized. These wavelengths are indicated with arrows in Figure 4. The SC values of 20.2 dB and 18.0 dB at 1534 nm and 1585 nm, respectively, correspond to forward switching (indicated with red arrows). Reverse switching, marked with a yellow arrow, shows an SC of 19.2 dB at 1540 nm. The achieved switching contrast of up to 20 dB is comparable to that reported in [32]; however, in our case, it is maintained over a broader spectral range, confirming improved switching performance. The homogeneous spectral profile indicates effective switching of the entire signal pulse, in contrast to the previous study, where the extinction ratio,  $ER(\lambda, E_{in})$ , exhibited a strong peak shape and vanishing switching contrast at the spectral wings.

The required control pulse energy at a 14 mm DCF length is in close correspondence with the theoretical value derived from the concept of the nonlinear balancing of DC asymmetry. This calculation considered an effective mode area of  $1.41 \mu\text{m}^2$  in one fiber core, a pulse duration of 270 fs, and an in-coupling efficiency of 50% [35], resulting in a control pulse energy of 0.76 nJ [32]. An important advantage of the lower switching energy is the reduced nonlinear distortion of the control pulse, which impacts the spectral content

of the signal pulse via cross-phase modulation. The different group velocities at 1030 nm and 1560 nm cause a variation in the overlap of the two pulses during co-propagation, influencing the shape of the signal pulse. However, such distortions are markedly reduced at lower control pulse energies, ensuring the advantageous homogeneous switching picture across the signal pulse spectra presented in Figure 4.

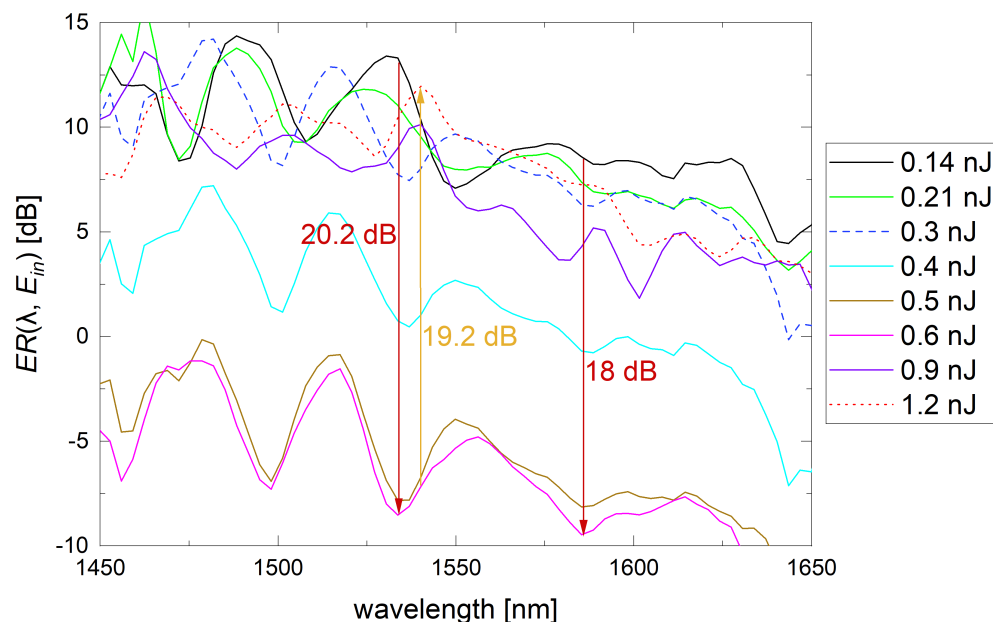


**Figure 4.** Spectrally resolved DC extinction ratio,  $ER(\lambda, E_{in})$ , measured in the same experimental conditions and at the same energy levels as in the case of camera registrations presented in Figure 3 (first generation DCF). The three arrows indicate the selected wavelengths with extreme switching contrast: 1534 nm/20.2 dB and 1585 nm/18 dB between energy values 0.14–0.6 nJ (cross-switching) and 1540 nm/19.2 dB between 0.6–1.2 nJ (reversal switching).

### 3.2. Delay Dependence

To analyze the effect of a temporal overlap between the signal and control pulses, we recorded a series of images of the fiber output facet at different positions of the delay line unit placed into the control pulse arm. The camera images of the fiber output were recorded under the same experimental conditions as during the series presented in Figure 3 while keeping the energy of the control pulse at the optimal 0.6 nJ level. The control pulses were sequentially delayed in relation to the signal one by steps of 66.7 fs.

Figure 5 reports the images collected at different delays. The optimal delay point at which the energy dependence was recorded (Figure 3) is marked as 0, and the new image series was collected in the range of  $\tau$ : (−400.3–333.6 fs). We again observed a reversal exchange of the dominant core: (i) the top (excited) core to the bottom (cross) one between −400.3 and 0 fs; (ii) reversal switching from the bottom to top cores between 0 and 266.8 fs. Figure 6 illustrates the  $ER$  dependence on the delay constructed via the processing of the camera images, which reveals a monotonic increase in  $ER$  with an increasing absolute value of the delay. Due to the instantaneous character of Kerr nonlinearity, the most efficient transfer to the cross core, with an  $ER$  of −7 dB, occurred at 0 delay. This represents the initial delay, ensuring the maximal cumulative overlap between the control and signal pulses during co-propagation and resulting in a maximal signal pulse cross-transfer. The delay dependence is slightly asymmetric, expressing higher DC extinction ratios with a positive  $\tau$ . This observation suggests that the self-steepening process degraded the control pulse, leading to a steeper change in the extinction ratio at positive delays.

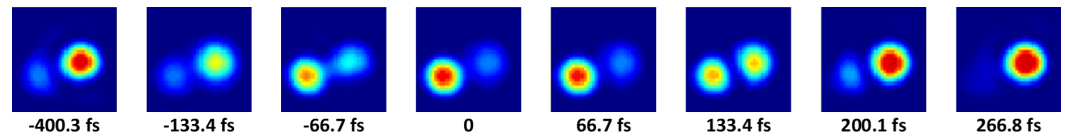


**Figure 5.** Infrared camera images of the output field of the 1560 nm, 75 fs signal pulse at 14 mm DCF with cross section as shown in Figure 1 under increasing delay of 1030 nm, 270 fs control pulse with energy of 0.6 nJ.

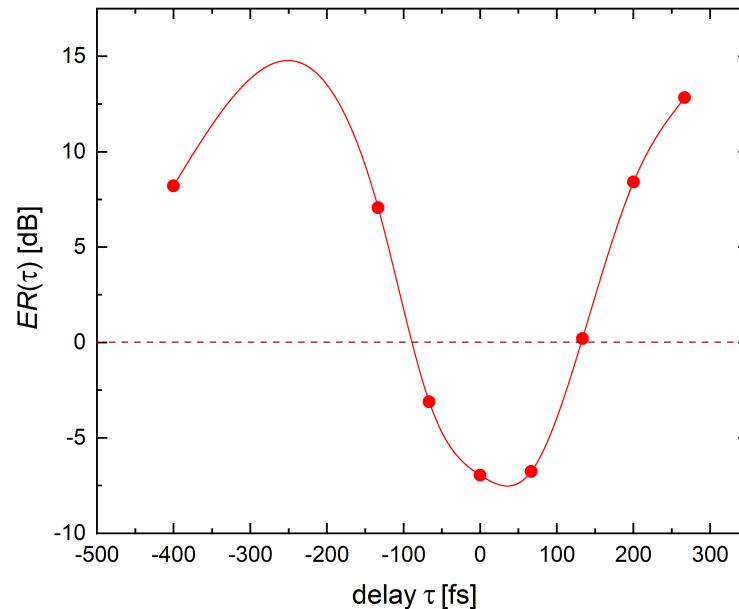


**Figure 6.** Dependence of the  $ER$  as a function of the control pulse delay in the range of  $\tau$  :(-400.3–333.6 fs) in the case of DCF with length 14 mm under excitation by 1030 nm, 270 fs control pulses with 0.6 nJ energy. The solid red line is a guide to the eye, obtained by interpolating the discrete experimental points using a predictive model to facilitate readability.

Simultaneously with the camera registrations, the output spectra originating from both cores were recorded and processed as described in the previous section and are presented in Figure 7. The spectrally resolved  $ER$  confirms the same switching performance observed in the camera image series, with curves ranging from  $-66.7$  to  $66.7$  fs consistently located in the negative half at the majority of wavelengths of the displayed spectral range (1450–1650 nm). Notably, there are three wavelengths at which the SC exceeds 10 dB: (i) at 1488 nm between  $-400.3$  and  $66.7$  fs, representing the first switching (red arrow), (ii) at 1534 nm between  $66.7$  fs and  $266.8$  fs, representing reversal switching (yellow arrow), and (iii) at 1560 nm between  $0$  and  $266.8$  fs, again representing reversal switching (yellow arrow).

### 3.3. Dual-Core Asymmetry Effect

The effect of DC asymmetry on the dual wavelength switching performance was analyzed using another fiber belonging to a second generation of DCFs (SG-DCF) series. In accordance with the calculated effective refractive indices presented in [35], the fiber has lower asymmetry with  $\delta_a = 1.2 \cdot 10^{-4}$  at 1560 nm. It was achieved thanks to the more precise control of the pulling and seeding speeds of the fiber during the fabrication process and applying more layers of UV-710 glass capillaries around the central PBG-08 cores [36,37]. Moreover, the second-generation DCF contains five DC units. A geometric analysis revealed that the central unit exhibits the highest degree of symmetry; therefore, it became the primary focus of our study.

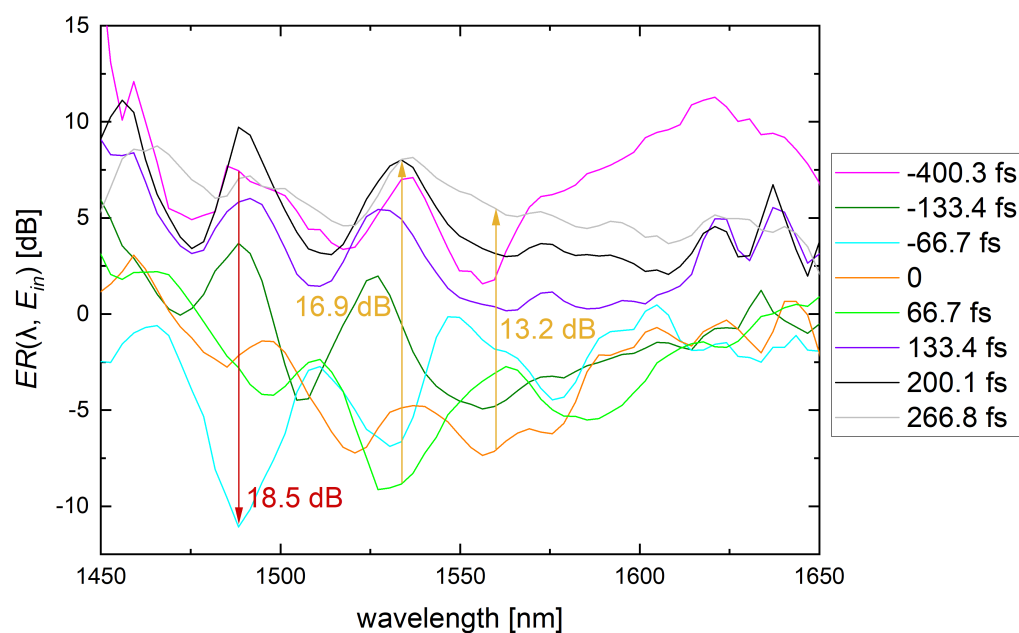


**Figure 7.** Spectrally resolved extinction ratio  $ER(\lambda, \tau)$  obtained from processing the output spectra measured at delays at 0.6 nJ energy in the same experimental conditions as in the case of the camera registrations presented in Figures 5 and 6. The three arrows indicate the selected wavelengths with extreme SC: 1488 nm/18.5 dB between  $-400.3$  and  $-66.7$  fs (first switch), 1534 nm/16.9 dB between 66.7 and 266.8 fs, and 1560 nm/13.2 dB between 0 and 266.8 fs (back switch).

The experimental setup and data acquisition process was the same as that described in the previous section. Figure 8 shows the dependence of MER on the fiber length,  $L$ , for the second-generation DCF under fiber length reduction by cutting back from 30 mm to 14 mm. In contrast to the results obtained for the FG-DCF (presented in Figure 2), in this case, MER is negative only at three fiber lengths (at 24, 22, and 18 mm), revealing that the switching does not take place across the entire length range analyzed. The extreme MER value of  $-8.7$  dB was obtained at the fiber length of 22 mm, which is comparable to the  $-9.1$  dB obtained for the 14 mm FG-DCF (Figure 2). As confirmed through our numerical simulations considering artificially symmetric structures, the length difference is caused by a slightly larger distance between the core centers in the SG-DCF (3.3 vs. 3.2  $\mu\text{m}$ ), which leads to an elongation of the coupling length [33].

Thus, the experimental study of both DCFs confirms the relation of dual-wavelength switching performance to the nonlinear balancing of DC asymmetry, which is our theoretical concept. Figure 9 shows the camera image at the output of the SG-DCF with an optimal length of 22 mm. Due to the lower level of  $\delta_a$  (i.e., a lower difference between the refractive indices of the fast and slow cores), a noticeable amount of the signal pulse energy was transferred to the cross-core already in the linear propagation regime. This resulted in a lower level of the DC extinction ratio at a control pulse energy of 0.14 nJ. With increasing energy, switching from the excited core to the cross-core was achieved at a control pulse energy of 0.4 nJ and maintained with high contrast up to the energy of 1.2 nJ. The cross-core dominance was reversed, starting from 4 nJ control pulse energies. Therefore, similar to the case of FG-DCF (Figure 3), cross and reversal switching steps were observed, albeit at different energy levels.

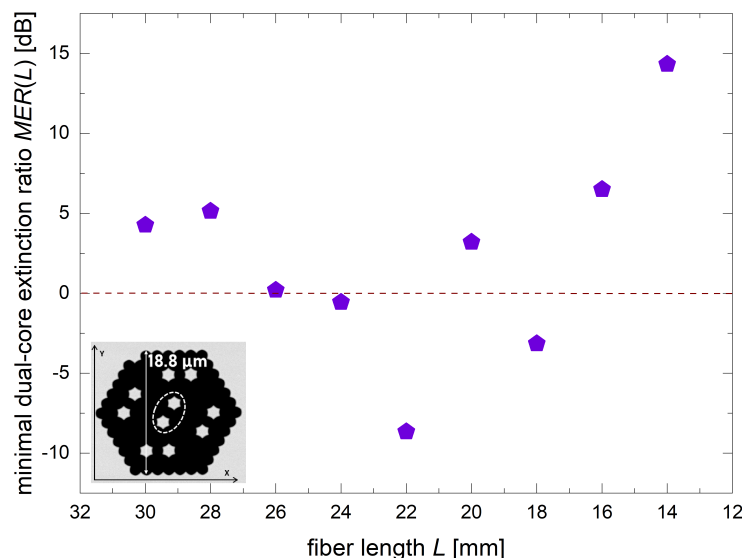


**Figure 8.** Dependence of the MER for each analyzed length of the SG-DCF with improved DC symmetry and cross section as inset.

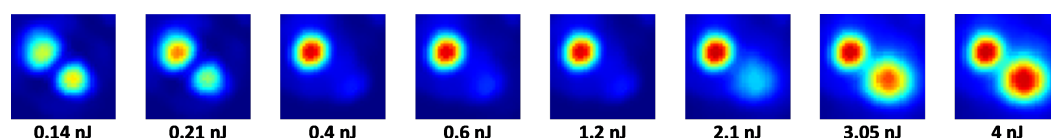


**Figure 9.** Infrared camera images of the output field of the 1560 nm, 75 fs signal pulse at 22 mm of the SG-DCF with cross section as shown in Figure 8 under increasing energy of 1030 nm, 270 fs control pulses.

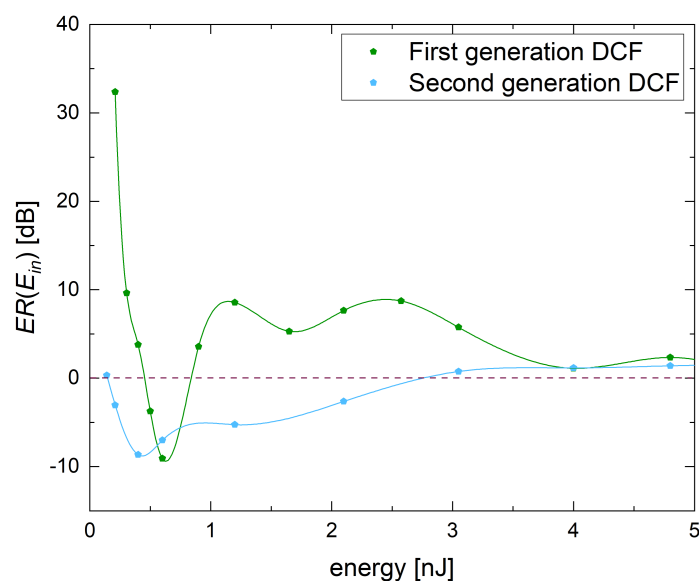
### 3.4. Comparison of the Switching Performance of the Two DCFs

Figure 10 summarizes the energy dependence of the  $ER$  at the optimal fiber lengths (14 mm and 22 mm) for the FG-DCF and the SG-DCF, which exhibit different levels of asymmetry. For SG-DCF, the difference between the effective refractive indices of the two cores,  $\delta_a$ , is approximately half that of the FG-DCF, suggesting a reduced energy requirement for the balancing control pulse. However, in agreement with theoretical predictions [38], lower asymmetry leads to higher linear coupling efficiency, which results in reduced  $ER$  at both low and high control pulse energies, even at the optimal fiber length.

These theoretical predictions were confirmed by comparing the energy dependence of  $ER$  in Figure 10. Approximately half the control pulse energy was required for switching in the SG-DCF relative to the FG-DCF. However, the MSC was four times higher in the FG-DCF. Despite the differences in switching performance, theory predicts similar MER values for both fibers, which aligns with our experimental observations. This similarity is attributed to the fact that the same effective symmetry level can be achieved through nonlinear balancing when identical control and signal pulses propagate under similar conditions in both fibers.

A particularly advantageous asymmetry level of  $\delta_a = 2.2 \cdot 10^{-4}$  was identified in the FG-DCF, where a notably high MSC of 41.6 dB was achieved. While further increasing the asymmetry could enhance switching contrast, it would also raise the control energy requirement, potentially eliminating the sub-nanojoule operation regime. Thus, the FG-DCF represents a near-optimal configuration for dual-wavelength switching at the applied wavelengths. It is important to note that the asymmetry in the effective refractive index is wavelength-dependent, so the optimization described here is specific to operation within the C-band. The advantages of the FG-DCF were also evident in the spectral domain: MSC values exceeding 20 dB were observed exclusively in this fiber (see Figure 3). The only

significant drawback is its higher control pulse energy requirement compared to the SG-DCF. However, this can be mitigated by minimizing the walk-off between the signal and control pulses. Our numerical simulations indicate that reducing this walk-off would require redesigning the DC structure, introducing more degrees of freedom to the ratio between the core diameter and the inter-core gap. For both the studied photonic crystal fibers (PCFs), this ratio was approximately 1, which enables the following: (i) a simplified fabrication process using identical diameters for both core and cladding glass rods during stacking, and (ii) symmetry levels that facilitated the breakthrough experimental results reported in [33,39]. The calculated temporal walk-off for the FG-DCF is 152 fs [32], which is significantly smaller than the control pulse duration of 270 fs. Therefore, considering all the factors discussed above, we evaluate the FG-DCF as a nearly optimal structure for sub-nanojoule dual-wavelength all-optical switching.



**Figure 10.** Dependence of the  $ER$  as a function of the control pulse energy in the range of 0.14–5 nJ in the cases of FG- (green points) and SG- (blue points) DCF with optimal lengths 14 and 22 mm, respectively. The solid lines connecting the experimental points are obtained via interpolation using a predictive model to highlight trends and improve visualization.

Furthermore, the spectral profiles of the switching performance for the FG-DCF, as presented above, support this conclusion. The spectrally resolved extinction ratio maintains its sign across the entire examined spectral range of 1450–1650 nm at specific control pulse energies and time delays between the control and signal pulses (Figures 4 and 7). This behavior indicates a minimal distortion of the signal pulses at the fiber output—representing a significant improvement over our previous study—and further enhances the application potential of DCFs. The dependence of the DC  $ER$  on the delay between the signal and control pulses, shown in Figures 5 and 6, highlights the critical importance of temporal synchronization for achieving efficient switching. As previously suggested in [32], it was initially expected that optimal synchronization would correspond to maximum pulse overlap at the midpoint of the optimized fiber length, near the coupling length  $L_c$ . However, our recent findings show that the highest switching performance is achieved at fiber lengths slightly beyond  $L_c$ , likely due to a nonlinear distortion of the control pulse during co-propagation.

Despite this deviation, the flat  $ER$  observed across the spectral domain confirms minimal distortion of the signal pulse at the fiber output, underscoring the robustness of our approach for ultrafast all-optical signal processing. The demonstrated homogeneous spec-

tral response also reveals the potential for cascading such switching devices to repeatedly process the same signal pulse.

#### 4. Conclusions

In this work, we investigated femtosecond dual-wavelength switching performance using soft-glass dual-core fibers (DCFs) operating in the C-band of optical communication systems. For the first time, DCFs with varying levels of core asymmetry are examined and compared. The comprehensive study included an analysis of the effects of fiber length, control pulse energy, and the delay between the signal and control pulses. The switching was characterized by calculating the MER and the MSC at different fiber lengths and control pulse energies. The presented findings reveal that the asymmetry level of  $\delta_a = 2.2 \cdot 10^{-4}$  in the case of the FG-DCF is nearly optimal for the advantageous switching performance. Specifically, the FG-DCF achieved a remarkable switching contrast of 41.6 dB over a 14 mm length with a switching energy of 0.6 nJ, demonstrating sub-nanojoule-level switching performance. In comparison, the SG-DCF with  $\delta_a = 1.2 \cdot 10^{-4}$  exhibited a lower switching contrast of 10.7 dB over a 22 mm length, but it required a lower switching energy of 0.4 nJ. These results confirm that the switching mechanism is governed by the nonlinear balancing effect of DC asymmetry, where the control pulse elevates the effective refractive index in the fast core, thus enabling efficient signal pulse switching. As confirmed through our numerical simulations of artificially symmetric structures, the observed length difference arises from the slightly larger core-to-core distance in the SG-DCF (3.3  $\mu\text{m}$  vs. 3.2  $\mu\text{m}$ ), which results in an elongation of the coupling length. The numerical calculations yielded coupling lengths of 13 mm [32] and 21 mm [39] for the first- and second-generation DCFs, respectively, which are in good agreement with the experimentally determined optimal lengths of 14 mm and 22 mm reported in our recent study. The results presented here demonstrate the high potential of dual-wavelength switching for ultrafast all-optical signal processing, offering sub-nJ control energy requirements, short fiber lengths, and simpler fabrication compared to other cross-connect switching alternatives. The improved experimental study resulted in an already homogeneous spectral picture of the switching performance across the 1450–1650 nm spectral range, overcoming the pilot report about this novel approach [32]. This represents a significant step forward, increasing the application potential for simultaneously switching wavelength-division-multiplexed signal pulses that are precisely synchronized across the C-band. While the cascaded utilization of the DCF-based dual-wavelength switching scheme would still require several technical challenges to be addressed, a single switch can already be applied for optical buffering. This is achieved by redirecting the signal pulse into a closed fiber loop in the first step and dropping it out in the second step using properly synchronized control pulses. This potential application has already been experimentally verified, demonstrating comparable switching performance, regardless of whether the signal pulse is coupled into the excited or non-excited core relative to the control pulse input core [40]. An even more promising application was demonstrated through the sequential switching of a single signal pulse using a THz-repetition-rate series of control pulses, effectively mimicking an ultrafast time-resolved signal sequence [41]. The switched signal successfully transferred the time-dependent energy information to the cross core, enabling the single-shot measurement of such ultrafast pulse trains. Our current work is focused on the synchronized excitation of the DCF with a chirped signal pulse whose duration matches the temporal width of the control-pulse sequence. This approach would allow time-resolved, single-shot measurements by simply recording the switched signal field with a spectrometer. Thanks to the very low signal distortion, even the cascaded utilization of the DCF-based dual-wavelength switching scheme appears feasible once the remaining technical challenges are addressed. Future improvements could focus

on the utilization of an Er-doped fiber oscillator with dual outputs at 1560 and 780 nm as a source of synchronized control signal pulses to greatly simplify the system design. The simultaneous redesigning of the fiber for the new wavelengths with the minimization of the control-signal walk-off could introduce new conditions in terms of the device length, switching energy, and signal pulse preservation with practical significance already in the area of optical communication technologies.

**Author Contributions:** Conceptualization, M.L. and I.B.; methodology, M.L. and I.B.; software, M.L.; validation, M.L., A.P. and I.B.; formal analysis, M.L. and I.B.; investigation, M.L., I.A. and I.B.; resources, I.A., A.P., A.B., R.B. and I.B.; data curation, M.L. and I.B.; writing—original draft preparation, M.L. and I.B.; writing—review and editing, M.L., A.P., A.B., R.B. and I.B.; visualization, M.L.; supervision, A.P., A.B., R.B. and I.B.; project administration, M.L., A.P., A.B., R.B. and I.B.; funding acquisition, M.L., R.B. and I.B. All authors have read and agreed to the published version of the manuscript.

**Funding:** This research was funded in part by the Austrian Science Fund (FWF) [10.55776/15453] and the National Science Center, Poland [projects PRELUDIUM 17 2019/33/N/ST7/03142, CEUS-UNISONO 2020/02/Y/ST7/00136]. For open-access purposes, the author has applied a CC BY public copyright license to any author-accepted manuscript version arising from this submission.

**Data Availability Statement:** Data underlying the results presented in this paper are not publicly available at this time but may be obtained from the authors upon reasonable request.

**Acknowledgments:** M.L. acknowledges the program of financial support for foreign trips of doctoral students of the University of Warsaw for research and teaching purposes (ZIP—II turn) for supporting his lab work at TU Wien. Open Access Funding by TU Wien.

**Conflicts of Interest:** Author Ignas Astrauskas was employed by the company Light Conversion. The remaining authors declare that the research was conducted in the absence of any commercial or financial relationships that could be construed as a potential conflict of interest.

## Abbreviations

The following abbreviations are used in this manuscript:

DC	Dual-Core
DCF	Dual-Core Fiber
ER	Extinction Ratio
FG-DCF	First-Generation Dual-Core Fiber
$L_c$	Coupling Length
MER	Minimal Extinction Ratio
MSC	Maximal Switching Contrast
PBG-08	Lead Silicate Glass
PCF	Photonic Crystal Fiber
SC	Switching Contrast
SEM	Scanning Electron Microscope
SG-DCF	Second-Generation Dual-Core Fiber
UV-710	Borosilicate Glass

## References

1. Willner, A.E.; Khaleghi, S.; Chitgarha, M.R.; Yilmaz, O.F. All-Optical Signal Processing. *J. Light. Technol.* **2014**, *32*, 660–680. [[CrossRef](#)]
2. Agrell, E.; Karlsson, M.; Chraplyvy, A.R.; Richardson, D.J.; Krummrich, P.M.; Winzer, P.; Roberts, K.; Fischer, J.K.; Savory, S.J.; Eggleton, B.J.; et al. Roadmap of optical communications. *J. Opt.* **2016**, *18*, 063002. [[CrossRef](#)]
3. Melchert, O.; Brée, C.; Tajalli, A.; Pape, A.; Arkhipov, R.; Willms, S.; Babushkin, I.; Skryabin, D.; Steinmeyer, G.; Morgner, U.; et al. All-optical supercontinuum switching. *Commun. Phys.* **2020**, *3*, 146. [[CrossRef](#)]

4. Jie, L.; Olsson, B.E.; Karlsson, M.; Andrekson, P. OTDM add-drop multiplexer based on XPM-induced wavelength shifting in highly nonlinear fiber. *J. Light. Technol.* **2005**, *23*, 2654–2661. [[CrossRef](#)]
5. Li, J.; Olsson, B.E.; Karlsson, M.; Andrekson, P. OTDM demultiplexer based on XPM-induced wavelength shifting in highly nonlinear fiber. *IEEE Photonics Technol. Lett.* **2003**, *15*, 1770–1772. [[CrossRef](#)]
6. Brown, A.W.; Xiao, M. All-optical switching and routing based on an electromagnetically induced absorption grating. *Opt. Lett.* **2005**, *30*, 699–701. [[CrossRef](#)]
7. Morioka, T.; Saruwatari, M. All-optical ultrafast nonlinear switching utilizing the optical Kerr effect in optical fibers. *Opt. Eng.* **1990**, *29*, 200–209. [[CrossRef](#)]
8. Rostami, A.; Nejad, H.B.A.; Qartavol, R.M.; Saghai, H.R. Tb/s Optical Logic Gates Based on Quantum-Dot Semiconductor Optical Amplifiers. *IEEE J. Quantum Electron.* **2010**, *46*, 354–360. [[CrossRef](#)]
9. Roy, J.N.; Gayen, D.K. Integrated all-optical logic and arithmetic operations with the help of a TOAD-based interferometer device—alternative approach. *Appl. Opt.* **2007**, *46*, 5304–5310. [[CrossRef](#)]
10. Li, Z.; Chen, Z.; Li, B. Optical pulse controlled all-optical logic gates in SiGe/Si multimode interference. *Opt. Express* **2005**, *13*, 1033–1038. [[CrossRef](#)]
11. Li, Q.; Zhang, Z.; Li, D.; Zhu, M.; Tang, X.; Li, S. All-optical logical gates based on pump-induced resonant nonlinearity in an erbium-doped fiber coupler. *Appl. Opt.* **2014**, *53*, 8036–8042. [[CrossRef](#)] [[PubMed](#)]
12. Song, Y.; Chen, Y.; Jiang, X.; Liang, W.; Wang, K.; Liang, Z.; Ge, Y.; Zhang, F.; Wu, L.; Zheng, J.; et al. Nonlinear Few-Layer Antimonene-Based All-Optical Signal Processing: Ultrafast Optical Switching and High-Speed Wavelength Conversion. *Adv. Opt. Mater.* **2018**, *6*, 1701287. [[CrossRef](#)]
13. Dorren, H.; Hill, M.; Liu, Y.; Calabretta, N.; Srivatsa, A.; Huijskens, F.; de Waardt, H.; Khoe, G. Optical packet switching and buffering by using all-optical signal processing methods. *J. Light. Technol.* **2003**, *21*, 2–12. [[CrossRef](#)]
14. Jia, H.; Zhou, T.; Zhang, L.; Ding, J.; Fu, X.; Yang, L. Optical switch compatible with wavelength division multiplexing and mode division multiplexing for photonic networks-on-chip. *Opt. Express* **2017**, *25*, 20698–20707. [[CrossRef](#)]
15. Miao, W.; Yan, F.; Calabretta, N. Towards Petabit/s All-Optical Flat Data Center Networks Based on WDM Optical Cross-Connect Switches with Flow Control. *J. Light. Technol.* **2016**, *34*, 4066–4075. [[CrossRef](#)]
16. Yoshiki, W.; Tanabe, T. All-optical switching using Kerr effect in a silica toroid microcavity. *Opt. Express* **2014**, *22*, 24332–24341. [[CrossRef](#)]
17. Kieu, K.; Schneebeli, L.; Merzlyak, E.; Hales, J.M.; DeSimone, A.; Perry, J.W.; Norwood, R.A.; Peyghambarian, N. All-optical switching based on inverse Raman scattering in liquid-core optical fibers. *Opt. Lett.* **2012**, *37*, 942–944. [[CrossRef](#)] [[PubMed](#)]
18. Zhao, Y. All-optical power-controlled switching in four-wave mixing. *Opt. Lett.* **1989**, *14*, 1085–1087. [[CrossRef](#)]
19. Trillo, S.; Wabnitz, S. Coupling instability and power-induced switching with two-core dual-polarizations fiber nonlinear couplers. *J. Opt. Soc. Am. B* **1988**, *5*, 483–491. [[CrossRef](#)]
20. Betlej, A.; Suntsov, S.; Makris, K.G.; Jankovic, L.; Christodoulides, D.N.; Stegeman, G.I.; Fini, J.; Bise, R.T.; DiGiovanni, D.J. All-optical switching and multifrequency generation in a dual-core photonic crystal fiber. *Opt. Lett.* **2006**, *31*, 1480–1482. [[CrossRef](#)] [[PubMed](#)]
21. Rezaei, M.; Rochette, M. All-chalcogenide single-mode optical fiber couplers. *Opt. Lett.* **2019**, *44*, 5266–5269. [[CrossRef](#)]
22. Andrianov, A.; Sal'nikov, N.; Anashkina, E.A.; Dorofeev, V.V.; Motorin, S.E.; Sharafiev, A.R.; Timofeev, O.V.; Litvak, A.G. Nonlinear Optical Switching of Ultrashort Pulses in a Two-Core Tellurite Light Guide. *Optoelectron. Instrum. Proc.* **2025**, *61*, 12–18. [[CrossRef](#)]
23. Wysokiński, K.; Budnicki, D.; Fidelus, J.; Szostkiewicz, L.; Ostrowski, L.; Murawski, M.; Staniszewski, M.; Staniszevska, M.; Napierała, M.; Nasiłowski, T. Dual-core all-fiber integrated immunosensor for detection of protein antigens. *Biosens. Bioelectron.* **2018**, *114*, 22–29. [[CrossRef](#)]
24. Ribeiro, V.; Karlsson, M.; Andrekson, P. Parametric amplification with a dual-core fiber. *Opt. Express* **2017**, *25*, 6234–6243. [[CrossRef](#)]
25. Lian, Z.; Horak, P.; Feng, X.; Xiao, L.; Frampton, K.; White, N.; Tucknott, J.A.; Rutt, H.; Payne, D.N.; Stewart, W.; et al. Nanomechanical optical fiber. *Opt. Express* **2012**, *20*, 29386–29394. [[CrossRef](#)] [[PubMed](#)]
26. Papaioannou, M.; Plum, E.; Valente, J.; Rogers, E.T.F.; Zheludev, N.I. Invited Article: All-optical multichannel logic based on coherent perfect absorption in a plasmonic metamaterial. *APL Photonics* **2016**, *1*, 090801. [[CrossRef](#)]
27. Su, S.P.; Wu, C.L.; Cheng, C.H.; Huang, B.J.; Wang, H.Y.; Tsai, C.T.; Lin, Y.H.; Chi, Y.C.; Shih, M.H.; Lee, C.K.; et al. Nonstoichiometric SiC Bus/Ring Waveguide Based All-Optical Data Format Follower and Inverter. *ACS Photonics* **2016**, *3*, 806–818. [[CrossRef](#)]
28. Ono, M.; Hata, M.; Tsunekawa, M.; Nozaki, K.; Sumikura, H.; Chiba, H.; Notomi, M. Ultrafast and energy-efficient all-optical switching with graphene-loaded deep-subwavelength plasmonic waveguides. *Nat. Photonics* **2020**, *14*, 37–43. [[CrossRef](#)]
29. Hirooka, T.; Hirata, R.; Wang, J.; Yoshida, M.; Nakazawa, M. Single-channel 10.2 Tbit/s (2.56 Tbaud) optical Nyquist pulse transmission over 300 km. *Opt. Express* **2018**, *26*, 27221–27236. [[CrossRef](#)] [[PubMed](#)]

30. Ji, K.; Davidson, I.; Sahu, J.; Richardson, D.J.; Wabnitz, S.; Guasoni, M. Mode attraction, rejection and control in nonlinear multimode optics. *Nat. Commun.* **2023**, *14*, 7704. [[CrossRef](#)] [[PubMed](#)]
31. Ji, K.; Richardson, D.J.; Wabnitz, S.; Guasoni, M. Sub-nanosecond all-optically reconfigurable photonics in optical fibres. *Nat. Commun.* **2025**, *16*, 6665. [[CrossRef](#)]
32. Longobucco, M.; Astrauskas, I.; Pugžlys, A.; Pysz, D.; Uherek, F.; Baltuška, A.; Buczyński, R.; Bugár, I. High Contrast All-Optical Dual Wavelength Switching of Femtosecond Pulses in Soft Glass Dual-Core Optical Fiber. *J. Light. Technol.* **2021**, *39*, 5111–5117. [[CrossRef](#)]
33. Tai, L.X.T.; Longobucco, M.; Hung, N.V.; Pałuba, B.; Trippenbach, M.; Malomed, B.A.; Astrauskas, I.; Pugžlys, A.; Baltuška, A.; Buczyński, R.; et al. Analysis of high-contrast all-optical dual-wavelength switching in asymmetric dual-core fibers. *Opt. Lett.* **2024**, *49*, 149–152. [[CrossRef](#)]
34. Longobucco, M.; Cimek, J.; Čurilla, L.; Pysz, D.; Buczyński, R.; Bugár, I. All-optical switching based on soliton self-trapping in dual-core high-contrast optical fibre. *Opt. Fiber Technol.* **2019**, *51*, 48–58. [[CrossRef](#)]
35. Longobucco, M.; Cimek, J.; Pysz, D.; Buczyński, R.; Bugár, I. All-optical switching of ultrafast solitons at 1560 nm in dual-core fibers with high contrast of refractive index. *Opt. Fiber Technol.* **2021**, *63*, 102514. [[CrossRef](#)]
36. Longobucco, M.; Astrauskas, I.; Pugžlys, A.; Dang, N.T.; Pysz, D.; Uherek, F.; Baltuška, A.; Buczyński, R.; Bugár, I. Complex study of solitonic ultrafast self-switching in slightly asymmetric dual-core fibers. *Appl. Opt.* **2021**, *60*, 10191–10198. [[CrossRef](#)] [[PubMed](#)]
37. Pysz, D.; Kujawa, I.; Stępień, R.; Klimczak, M.; Filipkowski, A.; Franczyk, M.; Kociszewski, L.; Buźniak, J.; Haraśny, K.; Buczyński, R. Stack and draw fabrication of soft glass microstructured fiber optics. *Bull. Pol. Acad. Sci. Tech. Sci.* **2014**, *62*, 667–682. [[CrossRef](#)]
38. Agrawal, G.P. Chapter 2—Fiber Couplers. In *Applications of Nonlinear Fiber Optics*, 2nd ed.; Agrawal, G.P., Ed.; Academic Press: Burlington, NJ, USA, 2008; pp. 54–99. [[CrossRef](#)]
39. Nguyen, V.H.; Tai, L.X.T.; Bugar, I.; Longobucco, M.; Buczyński, R.; Malomed, B.A.; Trippenbach, M. Reversible ultrafast soliton switching in dual-core highly nonlinear optical fibers. *Opt. Lett.* **2020**, *45*, 5221–5224. [[CrossRef](#)] [[PubMed](#)]
40. Winkowski, M.; Longobucco, M.; Pysz, D.; Kujawa, I.; Buczyński, R.; Bugar, I. All-Optical Self-Switching of 1560nm Femtosecond Pulses in Highly Nonlinear Soft Glass Multicore Fiber. In Proceedings of the 2025 Conference on Lasers and Electro-Optics Europe & European Quantum Electronics Conference (CLEO/Europe-EQEC), Munich, Germany, 23–27 June 2025. [[CrossRef](#)]
41. Alex, S.P.; Winkowski, M.; Longobucco, M.; Kaksis, E.; Buczynski, R.; Pugžlys, A.; Baltuška, A.; Bugár, I. Ultrafast Cross-Switching of Long Wavelength Near-Infrared Pulses in Dual-Core Soft Glass Fibers for Time Gating of Spectroscopy Signals. In Proceedings of the 2025 Conference on Lasers and Electro-Optics Europe & European Quantum Electronics Conference (CLEO/Europe-EQEC), Munich, Germany, 23–27 June 2025. [[CrossRef](#)]

**Disclaimer/Publisher’s Note:** The statements, opinions and data contained in all publications are solely those of the individual author(s) and contributor(s) and not of MDPI and/or the editor(s). MDPI and/or the editor(s) disclaim responsibility for any injury to people or property resulting from any ideas, methods, instructions or products referred to in the content.